Energy Conversion and Management 76 (2013) 899–909

Contents lists available at ScienceDirect

Energy Conversion and Management

journal homepage: www.elsevier.com/locate/enconman

A modeling and control approach to advanced nuclear power plants with gas turbines

Günyaz Ablay *

Electrical & Electronics Engineering Dept., Abdullah Gül University, 38039 Kayseri, Turkey

ARTICLE INFO

Article history:
Received 13 June 2013
Accepted 27 August 2013

Keywords:
Nuclear reactor
Load following
Gas turbine
Load frequency control
Temperature control
Nuclear power plant
Modeling
Simulation

ABSTRACT

Advanced nuclear power plants are currently being proposed with a number of various designs. However, there is a lack of modeling and control strategies to deal with load following operations. This research investigates a possible modeling approach and load following control strategy for gas turbine nuclear power plants in order to provide an assessment way to the concept designs. A load frequency control strategy and average temperature control mechanism are studied to get load following nuclear power plants. The suitability of the control strategies and concept designs are assessed through linear stability analysis methods. Numerical results are presented on an advanced molten salt reactor concept as an example nuclear power plant system to demonstrate the validity and effectiveness of the proposed modeling and load following control strategies.

1. Introduction

Several advanced reactor concepts are under development to enhance the role of nuclear energy supply with manageable nuclear waste, effective fuel utilization, increased environmental benefits, competitive economics, recognized safety performance, and secure nuclear energy systems and nuclear materials [1,2]. Six most promising systems (Generation-4 reactors) have been selected by the GIF for further study to deal with the above challenges and provide new products such as hydrogen [3], sustainability compared to renewable energy [4], reduced nuclear wastes for disposal, and increased proliferation resistance: gas-cooled fast reactor (GFR), very-high-temperature reactor (VHTR), super-critical-water-cooled reactor (SCWR), sodium-cooled fast reactor (SFR), lead-cooled fast reactor (LFR), and molten salt reactor (MSR). Furthermore, small modular reactor (SMR) designs, which are based on current advanced reactors and the Generation-4 reactor concepts, can be economically viable for the energy needs of many countries in the world, for remote/isolated areas, and for specific applications (e.g. water desalination or heat production). The practicality and effective utilization of the above nuclear reactor concepts depend on sharing nuclear power with other power sources on the same electricity grid, which necessitates load following capabilities or plant-wide automatic control generations in nuclear power plants.

The goals for an effective plant-wide control system include automated control, safe and smooth process operation, and high-quality control in the face of disturbances. To achieve these goals, nuclear power plants can have base-load or open-loop (no recycle) and load-following or closed-loop (recycle) configurations. While both configurations have their own advantages and disadvantages, the modern design approaches are based on the closed-loop configurations. The open-loop configuration means that the units are arranged in series with no recycles so that the plant-wide control problem can be effectively broken up into the control of each individual unit operation. Since there is no feedback effects, the individual unit operations govern the dynamic behavior of the plant and the only path for disturbance propagation is linear along the process [5]. On the other hand, in the closed-loop configurations, the plant-wide control problem becomes much more complex because the presence of feedback significantly changes the dynamic and steady-state behaviors of the plant. The main feedback effects in a plant are described with overall time constant change and snowball effect [5,6]. The overall time constant can be different from the sum of the time constants of the individual units due to possible positive feedbacks. The snowball effect means that a small change in the plant input can produce a large change in plant output due to propagation around the feedback loop. These properties limit the control configurations in an integrated power plant. Therefore, a plant-oriented approach that uses heuristic rules

* Tel.: +90 352 224 8800; fax: +90 352 338 8828.
E-mail address: gunyaz.ablay@agu.edu.tr

0196-8904/$ - see front matter © 2013 Elsevier Ltd. All rights reserved.
http://dx.doi.org/10.1016/j.enconman.2013.08.048

based on plant understanding and experience is necessary for an effective plant-wide control in nuclear power plants.

In power plants, the power supply and demand must be balanced by either generation or load since transmission systems provide negligible energy storage [7]. The approaches for balancing power supply and demand utilize the load frequency control to provide inherent capability of load following. The current nuclear reactor technologies have adequate regulation margin and response capabilities for load following operations. The problem here is that the thermal generation systems often have difficulty in following the load due to the slow response of the units [8]. Hence, controlling dominant plant variables through local unit controllers can provide a general solution. Simple control strategies are desirable for complex plants in order to deal with overall feedback effects.

In the United States, nuclear power plants are mostly used as base-load units, providing efficiency economically and technically. However, an automatic load-following control mechanism to deal with the daily variations of power demand is necessary for countries with high nuclear shares or desiring to considerably increase carbon-free energy sources. For example, European Utility Requirements stipulate that reactors should be capable of daily load cycles from 20% to 100% of rated power. Some power plants in France and Germany have the capability to follow power changes in the range of 30–100% rated power [9,10]. Load following control studies for nuclear power plants have mostly been carried out in steam turbines due to prevalence of pressurized and boiling water reactors [10–20]. Recently, some studies have also been demonstrated for dynamic modeling, control and transient analysis in gas turbine nuclear plants [21–25]. Plant dynamics and control for super-light water and super-fast reactors have been studied in [26], and safety simulations in nuclear power systems based on computer codes have been collected in [27]. More detailed and complete models and control configurations have been provided for space nuclear reactors in [28,29]. On the other hand, the modeling and control studies of the gas turbine power systems have been given for thermal power plants other than nuclear power plants, such as fossil-fuel power plants. Many different types of gas turbines are currently in use in power systems worldwide [30–36]. In general, a typical model of the gas turbine consists of load–frequency control, temperature control and acceleration control loops [30]. The applicability of these control approaches to nuclear power plants requires a detailed study. Since there are no detailed nuclear plant models and control studies that consider gas turbine nuclear power plants, it is a significant necessity to develop control models for evaluating stability and feasibility of load following control approaches. Moreover, overall response of the nuclear power plants in terms of slow response of units and the snowball effect have not been taken into account yet, but these limiting effects must be studied for load following control systems.

The main purpose of the paper is to provide an overall plant-wide modeling and control approach for advanced nuclear plant plants with power generating gas turbines. Most of the modeling approaches for nuclear plants in the literature are based on mass-energy–momentum balances (mixture or two-fluid models) and thus, they are rather complicated and need many assumptions as well as calculations of many unmeasurable parameter values. On the other hand, the modeling approach in this study is based on lumped parameter models, i.e. first principles and physical laws of dominant systems as well as input/output models, which are simple and convenient to control, and simulation studies. Based on the proposed modeling approach, a control strategy is provided for a load following nuclear plant by considering temperature control of the reactor and load–frequency control of the turbine-generator systems. Simple and well-proven control strategies are designed for the next generation nuclear plants and overall stability analyses are provided for different plant-wide control strategies.

The research paper is organized as follows: Section 2 provides dynamic models for the nuclear plant systems. Sections 3 and 4 represent a plant-wide control design approach and numerical simulation results, respectively. The conclusion of this research is given in Section 5.

2. Dynamic modeling of nuclear power plants

State-of-the-art dynamic modeling of nuclear power plants requires knowledge, approximations and realistic interpretations of the dynamic behavior of its subsystems. The modeling approach in this study is based on the lumped parameter models that include several assumptions, e.g. transients during close neighborhood of critical reactivity, incompressible flow, constant mass flow rates, constant heat capacity and heat transfer coefficients. The dynamic models are to be developed based on the reference nuclear power plant illustrated in Fig. 1, but the models would be applicable to different nuclear reactor designs that may or may not include secondary and tertiary loops. The nuclear power plant is composed of a nuclear reactor, heat exchangers and power conversion unit which utilizes closed-loop Brayton cycle as has been proposed for most high-temperature reactors. The dynamic models that are used to control and to simulate the nuclear power plant under consideration are given in the following subsections.

2.1. Mathematical modeling of nuclear reactors

The nuclear reactor is modeled by coupling neutronics with thermodynamics to capture the complexity of the physics of nuclear reactors. The reference scheme for modeling a nuclear reactor is given in Fig. 2. The nuclear reactor consists of neutronics and thermal modeling, temperature controller, control rod drive mechanism (governor) and hot/cold legs (in order to account for dynamic characteristics of pipeline) models.

Neutron flux or reactor power is calculated from point reactor kinetics equations (PRK) which assumes that the reactor transients are analyzed during slightly subcritical or supercritical reactor conditions.

$$\begin{aligned}\frac{dP(t)}{dt} &= \frac{\rho(t)-\beta}{\Lambda}P(t)+\sum_{i=1}^{6}\lambda_i C_i(t)\\ \frac{dC_i(t)}{dt} &= \frac{\beta_i}{\Lambda}P(t)-\lambda_i C_i(t)\end{aligned} \tag{1}$$

where $P(t)$ is the reactor power (in watts), $C_i(t)$ is the ith precursor or latent power (in Watts), $\rho(t)$ is the reactivity (in $\Delta k/k$), β_i is the delayed neutron faction of the ith group, β is total precursor group fraction $\beta = \beta_1 + \ldots + \beta_6$, Λ is the mean neutron generation time (in seconds), λ_i is the decay constant for the ith precursor (in 1/s).

For fuel-circulating (e.g. MSR) reactors, the residence time of the fuel outside the core should be included in the neutronics model. Then, the modified PRK equations for fuel-circulating reactors (MSRs) are given by [37]

$$\begin{aligned}\frac{dP(t)}{dt} &= \frac{\rho(t)-\beta}{\Lambda}P(t)+\sum_{i=1}^{6}\lambda_i C_i(t)\\ \frac{dC_i(t)}{dt} &= \frac{\beta_i}{\Lambda}P(t)-\lambda_i C_i(t)-\frac{1}{\tau_c}C_i(t)+\frac{1}{\tau_c}e^{-\lambda_i\tau_L}C_i(t-\tau_L)\end{aligned} \tag{2}$$

where τ_c is the transit time of the fuel salt through the core $\tau_c = m_c/\dot{m}$ (in seconds), τ_L is the transit time of the fuel through external loop $\tau_L = m_L/\dot{m}$ (in seconds), $\dot{m}$ is the total mass flow rate (in kg/s), $\dot{m}$ is the total mass of the fuel in the primary loop (in kg). For the precursor concentration dynamics (2), the third term in the

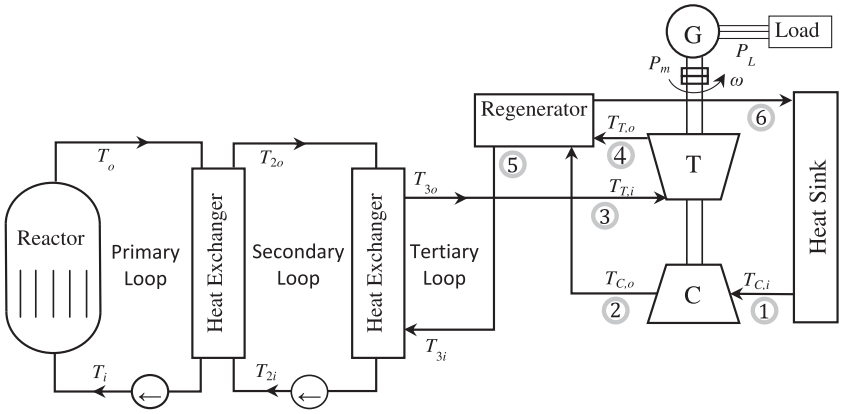

Fig. 1. Simplified scheme of an advanced nuclear power plant concept. It should be noted that depending on reactor types, nuclear reactors can also have one-loop or two-loop configurations.

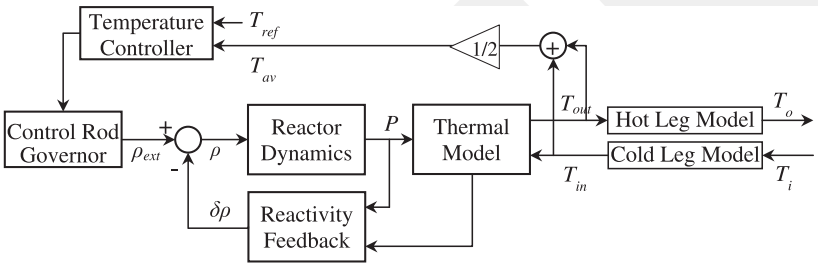

Fig. 2. A typical representation of nuclear reactor system and its average temperature control mechanism.

right-hand side accounts for the rate of delayed neutron precursors flowing out of the core, and the fourth term in the right hand side take into account the decay effects of the delayed neutron precursors flowing into the core during the circulation in the primary loop.

As well-known, the PRK equations can be reduced to two first-order differential equations via one group delayed neutron approach to ease calculations. This can be an option in numerical simulations since reactivity feedback makes the PRK nonlinear. The effects of temperature and density changes are primarily concerns in reactivity feedback [38]. Due to the relationship between density and temperature in fluids, the density variations can usually be expressed as a function of temperature, and thus a total temperature reactivity feedback can be considered. Then, the time dependency of reactivity $\rho(t)$ in (1) and (2) can be written as a function of external reactivity input, $\rho_{ext}(t)$, and the total temperature feedback [38,39]

$$\rho(t) = \rho_{ext}(t) - \alpha(T_{out} - T_r) \tag{3}$$

where T_{out} is the reactor outlet temperature (in °C), T_r is an equilibrium reference temperature (in °C), α is the total temperature feedback coefficient (in 1/°C).

Under constant thermal properties and mass flow rate $\dot{m}$, $T_{out}(t)$ can be found from

$$\begin{aligned} \frac{dT_{out}}{dt} &= k_f P(t) - \gamma_f (T_{out} - T_{in}) \\ P_{th} &= \dot{m} c_p (T_{out} - T_{in}) \end{aligned} \tag{4}$$

where k_f is the reciprocal of the reactor heat capacity $k_f = 1/m_c c_p$, $1/\gamma_f$ is the mean time for heat transfer $1/\gamma_f = m_c/\dot{m}$, c_p is the heat capacity coefficient (in J/kg °C), P_{th} is the thermal power generated by reactor (in watts), T_{in} is the reactor inlet temperature (in °C). The thermal power generated by the reactor (4) equals to the reactor power described in (1) or (2) under steady-state conditions.

The hot leg and cold leg temperature model can be included in the system modeling in order to handle the dynamic characteristics of the pipeline system where fluid loses energy due to friction. The dynamics of the pipeline together with control valves can act as a variable resistance and a simple capacity, which results in time delay in energy transfer systems [40]. The hot leg and cold leg models can simply be expressed with the following first order differential equations

$$\tau_{hl} \frac{dT_o}{dt} = -T_o + T_{out} \;\; \tau_{cl} \frac{dT_i}{dt} = -T_i + T_{in} \tag{5}$$

where τ_{hl} and τ_{cl} are the time constants (in seconds) for hot leg and cold leg temperature models, respectively.

Control rod governors (control rod drive mechanism) adjust the position of the control rod banks in the reactor core to obtain smaller incremental reactivity changes per step. While the reactivity control mechanism can consist of nonconventional methods, such as carbon reflector or shim gas, all types of reactivity control systems are addressed as control rod governors in this study. The control rod governor can simply be modeled with a first order differential equation as

$$\tau_g \frac{d\theta}{dt} = -\theta + \Delta V \tag{6}$$

where τ_g is the time constant of the rod drive mechanism (about several milliseconds), θ is the governor output position and ΔV is the governor input voltage. The output of control rod governor is then converted into reactivity input ρ_{ext} by the integral rod worth function [41] which is approximately given by

$$\rho(\theta) = \rho(H)\left(\frac{\theta}{H} - \frac{1}{2\pi}\sin\left(\frac{2\pi\theta}{H}\right)\right) \tag{7}$$

where θ is the axial distance and H is the total reactor core height. The average rod worth is used for control calculations in power

reactors due to critical reactor conditions, whereas in space reactors the rod worth is the function of stepper motor position [28].

2.2. Modeling flow control systems

The coolant flow rate at the rated power is controlled through reactor coolant pumps (or flow control valves). More specifically, the total mass flow rate is computed and compared with a reference flow rate, and a flow controller is designed to manipulate the flow control system [42,43]. The total mass flow of the coolant through the reactor when operating at rated power is given by

$$\dot{m} = \frac{P_{th}}{c_p \Delta T} \tag{8}$$

where ΔT is the difference between the reactor outlet and inlet temperature, and the flow rate has the units of cubic meter per hour (m^3/h) or tons per hour. To adjust the speed of the mass flow rate, electrical motor driven centrifugal pumps are commonly used in nuclear power plants. As shown in Fig. 3, the pump curve provided by the manufacturers shows the performance of pump, i.e. its head (H), flow rate ($\dot{m}$) and power (P). In pumping applications, variable frequency (or speed) drives are efficient flow control methods, together with throttling and bypass methods.

The basic formulation of the pump models is given by [44]

$$\frac{2\pi}{60} J \frac{dN(t)}{dt} = M_m - M \tag{9}$$

where N is the pump speed (in rpm), J is the pump moment of inertia (in kg m^2), M_m is the motor torque (in N m), M is the pump (hydraulic) torque (in N m).

The torque-power relation is given by $P = 2\pi NM/60$, where P is the power (in watts). The power characteristics of a pump are determined from pump curve and the affinity laws [44]. The affinity laws state that for a given pump, the flow rate varies directly as the speed, the head varies as the square of the speed, and the required electrical power varies as the cube of the speed. That is,

$$\dot{m} = k_1 N, \quad H = k_2 N^2, \quad P = k_3 N^3 \tag{10}$$

for some constant coefficients k_1, k_2 and k_3. For example, if speed changes from N_0 to N_1, then required power change will be $P_1 = P_0(N_1/N_0)^3$.

2.3. Dynamic modeling of the heat exchangers

Heat exchangers (HEXs) in nuclear power plants are used as auxiliary equipment which transfers heat from one fluid to another. A schematic diagram and a temperature profile of HEXs are shown in Fig. 4 in which a process fluid is heated on the tube side (cold stream) of the HEX by circulating hot fluid in the shell side (hot stream). The control approaches for HEXs are temperature control, cascade control, feedforward control and bypass control. The temperature control is the simplest approach, but the bypass control provides the fastest response [45]. In nuclear power

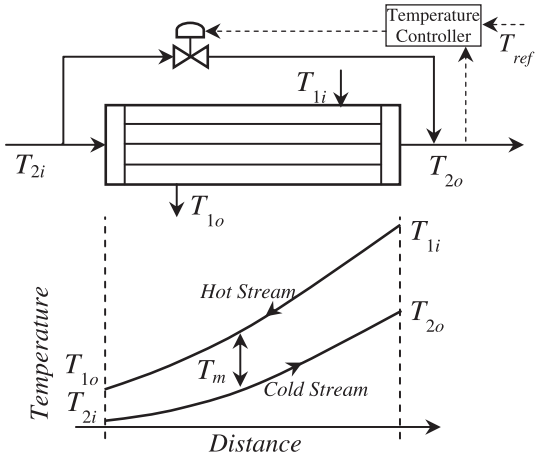

Fig. 4. A counterflow heat exchanger with a bypass control mechanism.

plants, the HEXs are used as process-to-process HEXs for heat recovery within a process. The bypass control can provide a simple and fast temperature control through cold stream bypassing as shown in Fig. 4. The bypass control is cost effective and minimizes the effects of exchanger dynamics in the loop so that the dynamic behavior of the HEX can be ignored because the flow control response is much faster than that of HEX [5,46].

Accurate models for HEXs contain partial differential equations which are rather complicated. For control and simulation aims, the low-order and well-approximated models can be obtained from the transfer function and state space approaches with first order differential equations mathematically [46]. A simple and approximately accurate HEX model with state-space representation is given by [47]

$$\begin{aligned} m_2 c_{p2} \frac{dT_{2o}}{dt} &= \dot{m}_2 c_{p2}(T_{2i} - T_{2o}) + UAT_m \\ m_1 c_{p1} \frac{dT_{1o}}{dt} &= \dot{m}_1 c_{p1}(T_{1i} - T_{1o}) - UAT_m \\ T_m &= \frac{(T_{1i} - T_{2o}) - (T_{1o} - T_{2i})}{\ln((T_{1i} - T_{2o})/(T_{1o} - T_{2i}))} \end{aligned} \tag{11}$$

and the steady-state thermal power balance is

$$P_{th} = C_f UAT_m \tag{12}$$

where m_1, m_2 are masses of the cold and hot streams (in kg), $\dot{m}_1$, $\dot{m}_2$ are flows of the hot and cold streams (in kg/s), c_{p1}, c_{p2} are heat capacities of cold and hot streams (in J/kg °C), U is the overall heat transfer coefficient (in watts/m^2 °C), A is the heat transfer area (in m^2), T_{1o}, T_{1i} are final and initial temperatures of the hot stream (in °C), T_{2o}, T_{2i} are final and initial temperatures of the cold stream (in °C), T_m is the logarithmic mean temperature difference (in °C), C_f is the correction factor (around 0.85–1 for most applications).

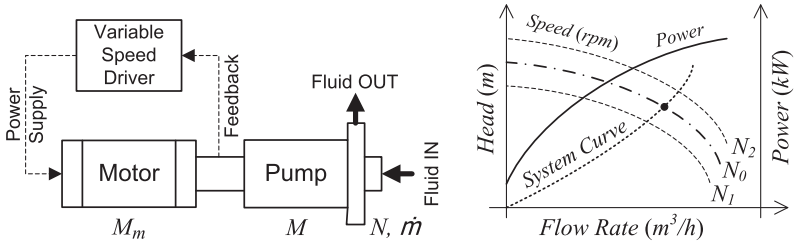

Fig. 3. Reactor coolant-pump system and pump curve.

In HEX model (11), the arithmetic mean temperature model can also be used for facilitating numerical calculations and simulations, which is given by [47]

$$T_m = \frac{1}{2}((T_{1i} - T_{2o}) + (T_{1o} - T_{2i})) \tag{13}$$

For controlling HEX, a proportional plus integral (PI) control (see Section 3) is usually adequate in most applications [5].

2.4. Dynamic modeling of gas turbine systems

In a gas turbine, stored energy of high temperature gas, originating from the nuclear reactor, is converted into mechanical energy, and then this mechanical energy is converted into electrical energy by the generator. The modern turbine units are in the form of tandem compound where all sections are on the same shaft with a single generator and run at 1800 rpm. The turbine power is adjusted through the control valve. The turbine controller manipulates the position of the control valves in order to control the fluid flow to the turbine so that the power output from the turbine is controlled. Fig 5 depicts the general structure of a gas turbine unit.

The energy balance is achieved through the closed-loop Brayton cycle with the temperature–entropy (T–s) diagram as displayed in Fig. 6. In Fig. 6, process (1–2) represents isentropic compression section, process (2–3) shows constant pressure heat addition section, process (3–4) displays isentropic turbine expansion, process (4–1) is for constant pressure heat rejection, and process (5–6) is showed to explain regeneration action to increase overall efficiency. The fluid is first compressed in an adiabatic process with constant entropy within the compressor (process 1–2). Then, it is heated with the power generated by the nuclear reactor which is transferred over heat exchangers (process 2–3). Next, the heated fluid is allowed to expand through the turbine (process 3–4). This gas expansion drives the turbine blades and consequently the shaft of the generator connected to it.

The ideal processes can be used to determine the compressor and turbine irreversible adiabatic efficiencies [48] from Fig. 6 as follows

$$\begin{aligned} \eta_C &= \frac{h_{2s} - h_1}{h_2 - h_1} \approx \frac{T_{2s} - T_1}{T_2 - T_1} \\ \eta_T &= \frac{h_3 - h_4}{h_3 - h_{4s}} \approx \frac{T_3 - T_4}{T_3 - T_{4s}} \\ \frac{T_{2s}}{T_1} &= \left(\frac{p_2}{p_1}\right)^{\frac{(\gamma-1)}{\gamma}} \equiv \frac{T_3}{T_{4s}} = \left(\frac{p_3}{p_4}\right)^{\frac{(\gamma-1)}{\gamma}} \equiv r \end{aligned} \tag{14}$$

where T is the absolute temperature (in K), h is the enthalpy (in kJ/kg), η_c is the compressor efficiency, η_T is the turbine efficiency, $p_2/p_1 = p_3/p_4$ is the cycle pressure ratio, γ is the constant specific heat ratio, and r is the isotropic temperature ratio.

In practice, since the compressor is operated in relatively constant thermodynamic conditions, but the turbine operation conditions change greatly, load and speed changes affect mostly the turbine efficiency [30,49]. Assuming that the quantities in (14) are constant, compressor and turbine outlet temperatures can be found as

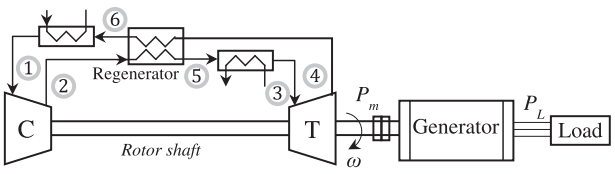

Fig. 5. A closed-loop Brayton cycle gas turbine system.

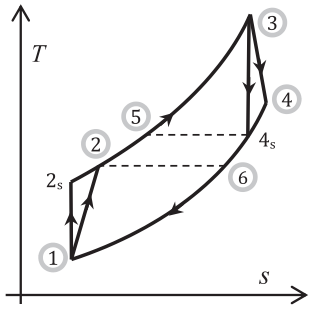

Fig. 6. The temperature–entropy (T–s) diagram of the Brayton cycle with ideal components and regeneration.

$$\begin{aligned} T_{C,o} &= (T_{C,i} + 273)\left(\frac{r-1}{\eta_C} + 1\right) - 273 \\ T_{T,o} &= (T_{T,i} + 273)\left(1 - \eta_T\left(1 - \frac{1}{r}\right)\right) - 273 \end{aligned} \tag{15}$$

where $T_{c,i}$ is the compressor inlet temperature (in °C), $T_{c,o}$ is the compressor outlet temperature (in °C), $T_{T,i}$ is the turbine inlet temperature (in °C), $T_{T,o}$ is the turbine outlet temperature (in °C).

Here, the compressor inlet temperature $T_{C,i}$ is assumed to be constant. By using (14) and (15), the overall power balance in the Brayton cycle is modeled with the following equations

$$\begin{aligned} P_T &= \dot{m}_g c_{p,g}(T_{T,i} - T_{T,o}) \\ P_C &= \dot{m}_g c_{p,g}(T_{C,i} - T_{C,o}) \end{aligned} \tag{16}$$

where P_T is the power produced by the turbine (in watts), and P_C is the power consumed by the compressor (in watts). The mass flow rate and specific heat capacity of circulating gas in the power conversion unit are $\dot{m}_g$ and $c_{p,g}$, respectively. From (16), the net mechanical power output can be modeled as

$$\tau_t \frac{dP_m}{dt} = -P_m + (P_T - P_C) \tag{17}$$

where P_m is the mechanical power (in watts) which drives the generator rotor shaft, and τ_t (in seconds) is the time constant for turbine system. The steady-state mechanical power is equal to

$$P_m = P_T - P_c$$

The synchronous generator unit converts the net mechanical power received from turbine into electrical power. The generator models are based on power balance and rotor speed of the generator. Naturally, any load changes in the power system result in deviations in the power balance. Suppose that a small change in load demand P_L causes a small deviation in the system speed (or frequency, f_o). Then, the generator-load balance equation is given by [50]

$$\frac{2H}{f_0}\frac{d\Delta f}{dt} + D\Delta f = P_m - P_L \tag{18}$$

where Δf is the frequency deviation, $\Delta f = f - f_o$ (in Hz), P_L is the change in demanded power (in megawatts), f_o is the synchronous (nominal) frequency (in Hz), H is the inertia constant, $H/P_o = J(2\pi f_o)^2/2P_o$ (about 2 to 9 s), J is the moment of inertia (in kg m^2), D is the load damping factor, $D = P_L/f_o$ (in megawatts per Hz). All types of composite load experience a change in power consumption with frequency so that speed measurement provides an efficient feedback control mechanism for power plants.

3. Control system design

The typical gas turbine models consist of three control loops: load frequency, temperature and accelerator controls [14]. The main control loop during normal operating conditions is the load frequency control. The other control loops, temperature and accelerator controls, are active in case of abnormal conditions. The acceleration control is used in the startup regime, which is ignored in this study. The reactivity input is limited with its predefined maximum and minimum limits. A control mechanism for the gas turbine nuclear reactors is illustrated in Fig. 7. The 'low value select' block is used to select different reactor power control signals, e.g. power control and average temperature control. The load frequency control is active during normal operating conditions, and uses speed deviation as input for control. On the other hand, when the temperature of the reactor exceeds the specified limit, the temperature control takes action.

3.1. Load frequency control

The frequency specification is satisfied when the power balance (18) is accomplished under steady state conditions. Any difference in power balance is instantly responded by a change in frequency (speed). The load frequency control is the main control mechanism during normal operating conditions [14,21]. The speed deviation between the measured and reference speed is the input of the load–frequency control. A number of sophisticated load frequency control methodologies have been studied in the literature [51]. Fig. 8 shows a typical load frequency control structure for power plants. The controller consists of primary (proportional) and secondary (integral) control loops.

The primary control loop uses the speed droop, R (in Hz/MW), which is proportional to generator output power. Speed droop is a governor function which reduces the governor reference speed as load increases [50]. The allowable speed range is 95–107% of the rated speed [10,30] which means that the typical value of R is around 4% of the nominal generator frequency in nuclear and thermal power plants. The secondary control loop for load frequency control can be designed as an integral control in order to handle steady-state frequency tracking error. By considering these controllers together, it is obvious that the load frequency controller is a proportional plus integral (PI) controller as follows.

$$\Delta P_c(t) = -\frac{1}{R}\Delta f(t) - K_i \int_0^t \Delta f(t)dt \tag{19}$$

where K_i is a constant integral control gain and R is the speed droop.

3.2. Temperature control

Temperature control is used in the gas turbine control mechanism to limit gas turbine output temperature at a maximum predetermined temperature [14]. In a nuclear power plant control, the temperature control is used to control the reactor output temperature when reactor temperature exceeds a constant maximum value. When the load demand increases, due to the load frequency control, the power output and, thus, the reactor temperature will increase. If this temperature is higher than the maximum rated reactor output temperature, the temperature control output will be lower than the load–frequency control output. Hence, the temperature control action will take over the control action.

Temperature control can also be designed as the PI controller for a deviation between reference and measured temperatures. The PI controller for the temperature control (which is represented in Laplace domain in Fig. 9) is given by

$$\Delta\rho(t) = K_p e(t) + K_i \int_0^t e(t)dt$$
$$e(t) = T_{ref} - T_{av} \tag{20}$$

where $e(t)$ is the error between the reference temperature and average reactor temperature, and K_p and K_i are the constant proportional and integral control gains, respectively. The average temperature is given by $T_{av} = (T_{out} + T_{in})/2$ for reactor inlet/outlet temperatures.

3.3. Model linearization and stability analysis

The system models of nuclear power plant can be represented with simple input/output models (transfer functions) for stability analysis. By considering system models described in Section 2, the simplified linear forms of these models are as follows. The rod control governor defined in (6) has the following transfer function

$$G_G(s) = \frac{1}{1+\tau_g s} \tag{21}$$

The nuclear reactor model for one group critical reactor without reactivity feedback is given by

$$G_R(s) = \frac{s+\lambda}{\Lambda s(s+\beta/\Lambda)} \tag{22}$$

This linear equation is an excellent approximation to reactor modeling, but do not include reactivity feedback. Nuclear reactors are inherently safe (stable) with reactivity feedback because they must be designed to have negative reactivity feedback, but without reactivity feedback the approximation (22) works for critical reactors. The stream legs (hot/cold legs) can be expressed as

$$G_L(s) = \frac{1}{1+\tau_l s} \tag{23}$$

where τ_l is the average time constant for legs. A good transfer function representation of HEXs is given by the first order plus dead time (FOPDT) model which is commonly used to design its temperature controller as follows,

$$G_H(s) = \frac{1}{1+\tau_h s} e^{-\theta s} \tag{24}$$

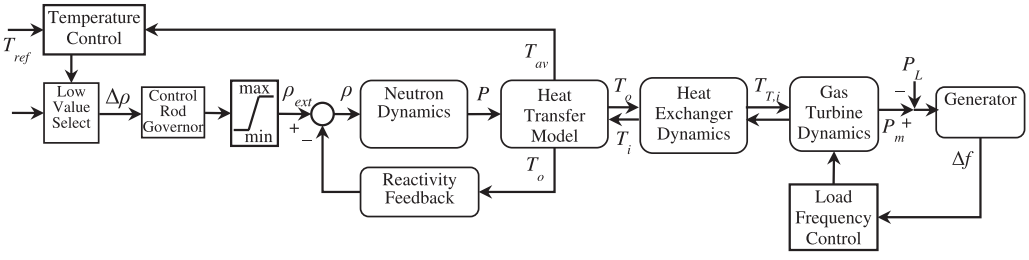

Fig. 7. A simplified illustration of the nuclear power plant and a load following control mechanism.

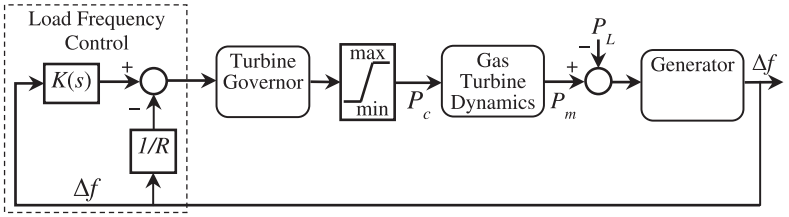

Fig. 8. Load frequency control mechanism.

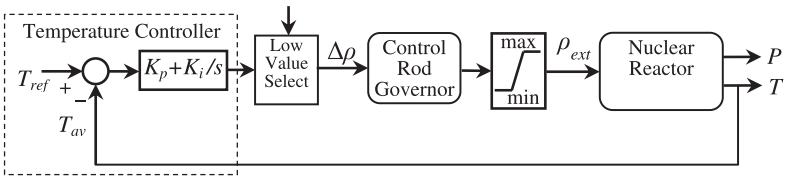

Fig. 9. Average temperature control system.

where τ_h is the time constant for HEX (around 5–120 s) and θ is the dead time (around 1–30 s) [46]. The approximate values of parameters τ_h and θ can be determined through process reaction curve approach. The time delay term can be approximated to $\exp(-\theta s) \approx 1/(1+\theta s)$ using Taylor series expansion. It should be noted that HEX dynamics may be ignored when it has a bypass control mechanism [5]. The turbine system can be expressed with

$$G_T(s) = \frac{1}{1+\tau_t s} \tag{25}$$

where τ_t (in seconds) is the time constant of turbine system. The generator-load model (18) has the following transfer function

$$G_{GL}(s) = \frac{1}{D+2Hs} \tag{26}$$

Now, stability of the control strategies can be analyzed with well-known linear stability theorems. Two different load-following control strategies are considered: load frequency control using control rod and turbine governors.

Case 1: Load frequency control mechanism using control rod governor. By using the above linear models, the block diagram of load frequency control mechanism can be obtained as illustrated in Fig. 10.

In Fig. 10, the $G_1(s)$ block represents all the series connected transfer functions, i.e.

$$G_1(s) = G_G(s)G_R(s)G_L(s)G_H(s)G_T(s) \tag{27}$$

and the $G_c(s)$ block represents the load frequency controller, i.e.,

$$G_c(s) = -\frac{1}{R} - K_i\frac{1}{s} \tag{28}$$

The closed-loop power plant system can be written as

$$f(s) = \frac{-G_{GL}(s)}{1-G_1(s)G_c(s)G_{GL}(s)}P_L(s) \tag{29}$$

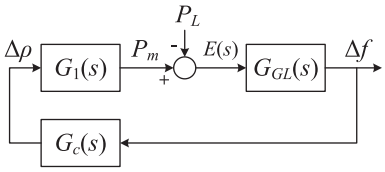

Fig. 10. A simplified closed-loop structure of a nuclear power plant.

While a positive feedback is seen in (29), the closed-loop system actually has a negative feedback due to negative sign of the controller $G_c(s)$ (see Eq. (28)). The characteristic polynomial of the closed-loop system is

$$1 - G_1(s)G_c(s)G_{GL}(s) = 0 \tag{30}$$

Substituting the system parameters into characteristic polynomial, we get

$$s(\Lambda s+\beta)G_c(s)\prod_{j=1}^{6}(1+\tau_j s) - \frac{1}{D}(s+\lambda) = 0 \tag{31}$$

For some appropriate parameter values in controller (28) and the typical system parameters values, it can be shown that the closed loop system is stable, i.e. real parts of the roots of characteristic polynomial of (31) are negative. The steady-state error of the controlled system can be determined from error function (see Fig. 10) as

$$E(s) = \frac{-1}{1-G_1(s)G_c(s)G_{GL}(s)}P_L(s) \tag{32}$$

The steady-error is then

$$\begin{aligned} e_{ss} &= \lim_{s\to 0} sE(s) \\ &= \lim_{s\to 0} s\frac{-s(\Lambda s+\beta)G_c(s)\prod_{j=1}^{6}(1+\tau_j s)}{s(\Lambda s+\beta)G_c(s)\prod_{j=1}^{6}(1+\tau_j s) - (s+\lambda)/D}P_L(s) \end{aligned} \tag{33}$$

Due to PI controller $G_c(s) = -(s/R + K_i)/s$, for a step load change $P_L(s) = 1/s$, the steady-state error is $e_{ss} = K_i/(K_i - \lambda/\beta D)$. However, the ramp load changes are only acceptable for nuclear power plants due to safety concerns. For a ramp change $P_L(s) = 1/s^2$, the steady-state error with PI controller is $e_{ss} \to \infty$. Thus, the PI controller is not appropriate for ramp load changes. On the other hand, a P-controller with some steady-state error might be considered.

Case 2: Load frequency control mechanism using turbine governor. From Fig. 10, the closed-loop power plant system can be written as

$$f(s) = \frac{-G_{GL}(s)}{1-G_1(s)G_c(s)G_{GL}(s)}P_L(s) \tag{34}$$

where the controller $G_c(s)$ is the same as (28), and the $G_1(s)$ block has the following form

$$G_1(s) = G_T(s) \tag{35}$$

The characteristic polynomial of the closed-loop system is

$$1 - G_T(s)G_c(s)G_{GL}(s) = 0 \quad (36)$$

Substituting the system parameters into characteristic polynomial, we get

$$s(1+\tau_t s)(D+2Hs) + K_i + s/R = 0 \quad (37)$$

The Routh–Hurwitz criterion can be used to evaluate stability of the closed-loop system. Since all the parameters, H, D, τ_t, R and K_i, are positive definite, the control system is stable for the following values of the integral control gain

$$0 < K_i < 1 + DR + \frac{2H}{\tau_t}(1+R) \quad (38)$$

The steady-error is then

$$e_{ss} = \lim_{s\to 0} s\frac{-s(1+\tau_t s)(D+2Hs)}{s(1+\tau_t s)(D+2Hs) + K_i + s/R}P_L(s) \quad (39)$$

For a step load change $P_L(s) = 1/s$, the steady-state error is $e_{ss} = 0$. For a ramp load change $P_L(s) = 1/s^2$, the steady-state error is $e_{ss} = D/K_i$. The PI controller is necessary and adequate to deal with the ramp load changes in nuclear plants. It should be noted that the derivative control can also be included in the controller (i.e. constructing PID controller) to improve transient performance and a better margin of stability for the closed-loop system.

It is possible to draw a comparison between the control strategies given in Case 1 and Case 2. A direct load following control through nuclear reactor (Case 1) includes dynamic responses of all the series connected system, which results in a slow response and small stability margin. On the other hand, a load following control through turbine governor (Case 2) has a fast response and large stability margin. For these reasons, it is concluded that (*i*) a direct reactor based load following control for multiple coolant loop plants results in low stability margin and high overall time constant, and (*ii*) local unit controllers improve stability and overall time constant. The effectiveness of the load following control using local controllers (Case 2) is illustrated in the following application.

4. Simulation results

In this study, an MSR concept is utilized to realize control and simulation of the advanced nuclear power plants. The MSR is one of the most promising concepts since the experiments from the molten salt breeder reactor (MSBR) in Oak Ridge National Laboratory and preliminary calculations of kinetic and dynamic characteristics of the new MSR concepts show high level of controllability and safety. Several MSR systems are being studied, including the deep burn MSR [52], thorium MSR [53], small MSR [54,55] and advanced high temperature MSR [56]. In an MSR, the fuel is dissolved in fluoride or chloride salt coolants, which circulates in the primary loop. The fuel temperature, fuel salt density, fission product poisons and delayed neutrons are the main elements that dominate reactor dynamics of the MSR during operation. The MSR concepts have several attractive characteristics: strongly negative Doppler feedback [57], negative expansion reactivity feedback of molten fuel fluoride/chloride fuel [52,58], and negligible xenon concentration level due to use of a sparging system [57]. By utilizing these attractive features of the MSRs, an efficient automatic load following control mechanism can be developed.

The molten salt actinide recycler and transmuter (MOSART) system [52] is selected as an example advanced nuclear power plant to work with. One possible arrangement of the simplified MOSART units is given in Fig. 1. The reactor core is designed to provide 2400 MW thermal power from transuranic burn-up. The fuel salt is the combination of molten 15LiF–27BeF_2–58NaF (in mole%) and trifluorides of actinides. The secondary salt used to transfer heat from primary loop to the secondary loop and to limit the tritium release is NaF–$NaBF_4$. The power conversion unit for the MOSART system has not been designed so far, but a closed-loop Brayton cycle power conversion system is the natural solution. For MATLAB/Simulink-based numerical simulations, the main parameters of the MOSART concept are given in Table 1 [52]. The delayed neutron precursor parameters of the MOSART concept which are calculated and verified with MCNP5/MCNPX codes via ENDF/B-V and ENDF/B-VI nuclear data libraries are given in Table 2.

Table 1
Basic parameters of the MOSART system [52].

Core diameter/height (m)	3.4/3.6
Thermal/electrical power (MW)	2400/1200
Core fuel salt mass flow rate, $\dot{m}$ (kg/s)	10,000
Core fuel salt mass, m (kg)	69,946
Fuel salt density, d (kg/m^3)	2.140
Heat capacity of fuel salt, c_p (J/kg/°C)	2.087
Core transit time, τ_c (s)	7
Loop transit time, τ_L (s)	3.94
Total temperature coefficient, α (pcm/°C)	−3.86

Fluid parameters for HEXs are given in Table 3. Although the first HEX values are taken from [52], the intermediate loop HEX and regenerator values are the results of mass and energy balances.

At steady state, Brayton cycle values are given in Table 4. It is assumed that the pressure ratio and the specific heat ratio are constant during simulation. For practical considerations, it is assumed that the turbine, compressor and regenerator have efficiencies of 92%, 85% and 98%, respectively, in the determination of inlet and outlet temperatures of the components through a conventional thermodynamic cycle analysis. The overall thermal efficiency is about 50% initially.

The parameters of control systems are determined through MATLAB's PID control tuning algorithm (based on frequency domain algorithm). The simulation results are given for the following two cases: constant and variable mass flow rates. The current load following operation regulations are based on European Utilities' Requirements. The acceptable power fluctuating in nuclear plants in response to load following is about ±5%P_{base} per minutes so that power increase rate should not exceed this limit [59]. However, the fossil-fuel power plants have a limit of up to 20%P_{base} per minutes. In the following simulations, the variations in the load demand and reference mass flow rate have been selected faster than that of current nuclear reactors in order to assess the performance of advanced reactors effectively.

Case 1: Constant mass flow rate. The numerical simulation results are illustrated in Figs. 11 and 12. As seen in Fig. 11, the average temperature control system brings the average reactor temperature to its reference temperature value 665 °C in a short time by using control rod drive mechanism. The total reactivity margins of the MSRs correspond to around 1000 pcm (or 0.01 $\Delta k/k$)

Table 2
Delayed neutron data.

Group	Decay constant, λ_i (1/s)	β_i/β	Delayed fraction, β_i
1	0.0128	0.0293	9.96e−5
2	0.0300	0.2507	8.52e−4
3	0.1103	0.1725	5.87e−4
4	0.3135	0.3832	1.30e−3
5	0.8634	0.1275	4.34e−4
6	1.3503	0.0368	1.25e−4
Total delayed neutron fraction, β:			3.40e−3
Neutron generation time, $\lambda\Lambda$ (s):			8.3e−6

Table 3
Fluid parameters in the heat exchangers.

Fluid parameters	Fuel salt	Secondary salt	Secondary helium	Tertiary helium
Fluid density, d (kg/m^3)	2140	1750	178.5	178.5
Fluid mass flow rate, $\dot{m}$ (kg/s)	10000	13858	4022	1652
Fluid mass, m (kg)	39376	10850	187	187
Heat transfer coefficient, UA (MW/°C)	167	167	167	167
Heat capacity of the fluid, c_p (J/kg/°C)	2087	1506	5189	5189
Inlet temperature, T_i (°C)	606	590	564	Table 4
Outlet temperature, T_o (°C)	725	711	684	Table 4

Table 4
Steady-state Brayton cycle values.

	Brayton cycle state points	Temperature (°C)
1	Compressor inlet	30
2	Compressor outlet	84
3	Turbine inlet	684
4	Turbine outlet	570
5	Regenerator low pressure exit	90.5
6	Regenerator high pressure exit	564
Pressure ratio, p_2/p_1		1.58
Specific heat ratio, γ		1.66
Cycle efficiency, η(%)		50%

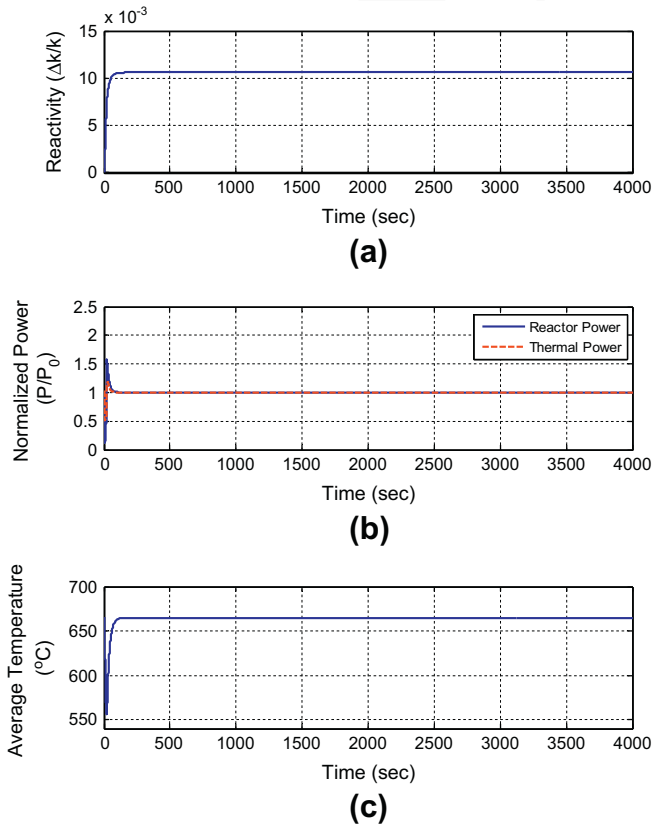

Fig. 11. Time responses for the average temperature control system, (a) reactivity provided by the control rod system, (b) normalized reactor power and extracted thermal power, (c) time response for average temperature.

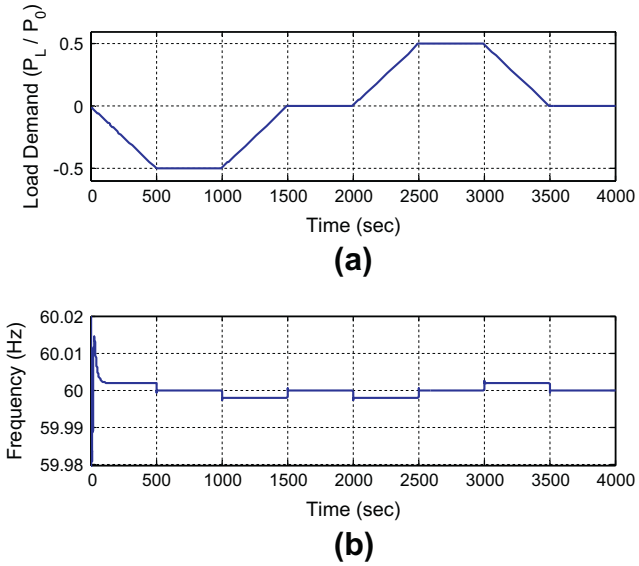

Fig. 12. Time responses for the load frequency control system, (a) load demand, (b) frequency variations.

reactivity addition in more than some minutes. The reactivity input is around 0.01 $\Delta k/k$ margin as seen in Fig. 11a. Since mass flow rate is constant, the reactivity, power and average temperature stays constant after short transients. In Fig. 12, the response of the load frequency control system is displayed. The load frequency control is obtained through turbine regulator during load power demand variations. The generator frequency is maintained around its reference value 60 Hz during load demand variations. Along ramp load changes, the generator frequency has a constant but small steady-state error as explained in Section 3.3. It can be observed that the load demand variations do not have visible effects (transients) on the average temperature control system. This can be explained with the fast response of the local unit controllers and slow response of the thermal systems (low pass filter properties of the thermal systems).

Case 2: Variable mass flow rate. The numerical simulation results are illustrated in Figs. 13–15. A reference mass flow rate of the primary loop is shown in Fig. 13. During the mass flow rate variations, the average temperature control system keeps the average reactor temperature around its reference value 665 °C through the control reactivity with some small transients as seen in Fig. 14. The reactivity input is around 0.01 $\Delta k/k$, which is compatible to MSR reactivity input limitation. In Fig. 15, the response of the load frequency control system is illustrated. Again, the generator frequency is maintained around its reference value 60 Hz during load demand variations. The variations in mass flow rate of the primary loop do not have a visible transient effect on the load frequency control system. This can again be explained with the fast response of the

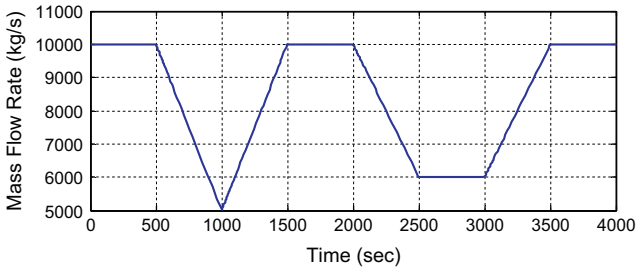

Fig. 13. Reference mass flow rate in the primary loop.

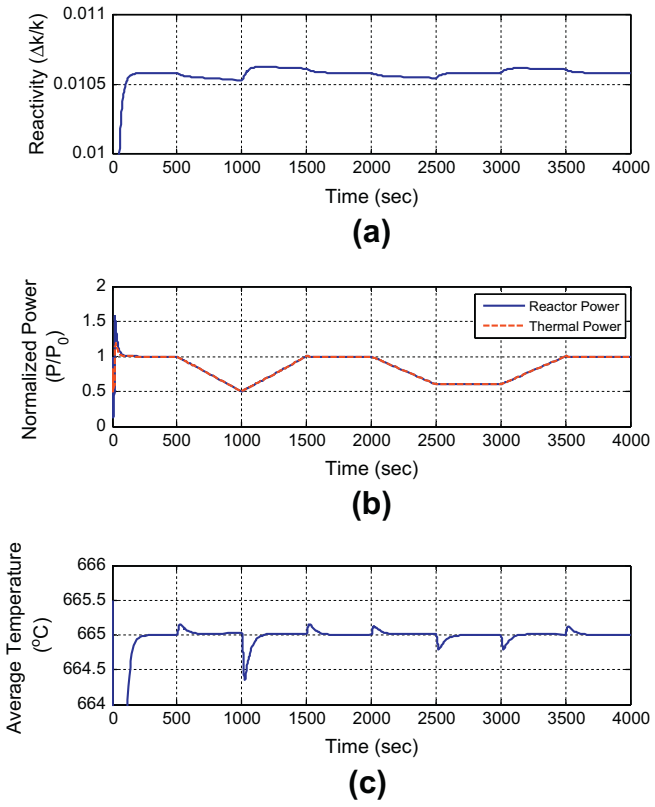

Fig. 14. Time responses for average temperature control system during mass flow rate variations, (a) external reactivity response, (b) normalized power and (c) average temperature.

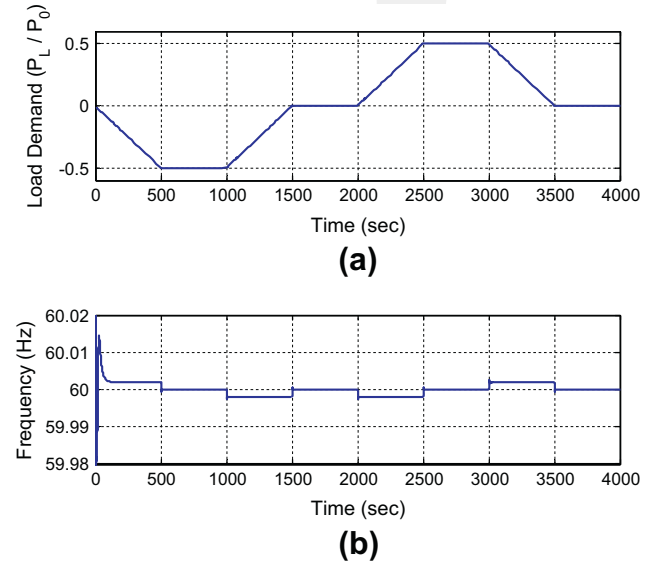

Fig. 15. Time responses for the load frequency control system during mass flow rate variations, (a) load demand and (b) frequency variations.

local unit controllers and slow back-response of the thermal systems.

5. Conclusion

Dynamic modeling and control problems of gas turbine nuclear power plants are investigated. The study set out to determine the effect of load following control strategies on the stability of advanced nuclear power plants. Load frequency control and temperature control strategies for a load following nuclear power plant are provided through simple dynamic models and well-proven controller designs. The complexity of the plant design (i.e. number of coolant loops) and the plant-wide control strategy (i.e. reactor-centered control or local unit controllers) have significant effects on stability and response time of the nuclear power plant. This research has shown that the effect of the load following in the pant-wide system control is twofold:

- Direct nuclear reactor-centered load following control for multiple coolant loops in the power plant results in low stability margin and long overall time constant,
- Local unit controllers improve stability and overall time constant.

Furthermore, the proposed modeling approach eliminates the limitations of complicated mixed or two-fluid models and allows us to design efficient control systems and to provide appropriate stability analysis. Since many components of power plants are similar, the proposed modeling and control approaches are applicable to various nuclear power plants, research reactors and space nuclear reactors with some minor modifications. The research might be extended to the model verification and validation using benchmark tests and to the interconnected power systems.

References

[1] DOE US. A technology roadmap for generation IV nuclear energy systems. U.S. DOE Nuclear Energy Research Advisory Committee and the Generation IV International Forum; 2002.
[2] Marques JG. Evolution of nuclear fission reactors: third generation and beyond. Energy Convers Manage 2010;51:1774–80.
[3] Torjman M, Shaaban H. Nuclear energy as a primary source for a clean hydrogen energy system. Energy Convers Manage 1998;39:27–32.
[4] Pappas C, Karakosta C, Marinakis V, Psarras J. A comparison of electricity production technologies in terms of sustainable development. Energy Convers Manage 2012;64:626–32.
[5] Luyben WL, Luyben ML, Tyreus BD. Plantwide process control. McGraw-Hill Professional Publishing; 1998.
[6] Rangaiah GP, Kariwala V. Plantwide control: recent developments and applications. John Wiley & Sons; 2012.
[7] Grigsby LL. Power system stability and control. CRC Press; 2007.
[8] Kundur P. Power system stability and control. McGraw-Hill Professional; 1994.
[9] Lokhov A. Load-following with nuclear power plants. NEA News 2011;29.2:18–20.
[10] OECD. Technical and economic aspects of load following with nuclear power plants. OECD, Nuclear Energy Agency; 2011.
[11] Bae IH, Na MG, Lee SH. Model predictive control for load-following operation of APR1400. Nuclear plant instrumentation, control, and human-machine interface technologies, Tennessee, USA; 2009.
[12] Chen D, Zhang D, Zhang Y, Jiang W. Study on modeling and control method of load-following for PWR nuclear power plant. Atom Energy Sci Technol 2010;44:321–4.
[13] Boroushaki M, Ghofrani MB, Lucas C, Yazdanpanah MJ. An intelligent nuclear reactor core controller for load following operations, using recurrent neural networks and fuzzy systems. Ann Nucl Energy 2003;30:63–80.
[14] Choi JI, Oh S, Song I, Hah Y, Kuh J, Lee U. Advanced load follow operation mode for Korean standardized nuclear power plants. J Kor Nucl Soc 1992;24:183–92.
[15] Dong Z, Feng J, Huang X. Nonlinear observer-based feedback dissipation load-following control for nuclear reactors. IEEE Trans Nucl Sci 2009;56:272–85.
[16] Na MG, Jung D, Shin S, Jang J, Lee J, Lee K. A model predictive controller for load-following operation of PWR reactors. IEEE Trans Nucl Sci 2005;52:1009–20.
[17] Eliasi H, Menhaj M, Davilu H. Robust nonlinear model predictive control for nuclear power plants in load following operations with bounded xenon oscillations. Nucl Eng Des 2011;241:533–43.
[18] Shinaishin MA, Sultan MA, El-Shaer HM, Rashad SM. Simulation of the dynamic performance of a PWR plant as a power supply in a large power system. IEEE Trans Nucl Sci 1981;28:923–8.
[19] Lam Wilson K. Advanced pressurized water reactor simulator – user manual; 2009.
[20] Das S, Pan I, Das S. Fractional order fuzzy control of nuclear reactor power with thermal–hydraulic effects in the presence of random network induced delay and sensor noise having long range dependence. Energy Convers Manage 2013;68:200–18.

[21] Wright SA. Dynamic modeling and control of nuclear reactors coupled to closed-loop Brayton cycle systems using SIMULINK. vol. 746, AIP; 2005. p. 991–1004.
[22] Moisseytsev A, Sienicki JJ. Automatic control strategy development for the supercritical CO_2 Brayton cycle for LFR autonomous load following. In: International congress on advances in nuclear power plants, ICAPP'06; 2006.
[23] Bortota S, Moisseytsevb A, Sienickib JJ, Artioli C. Core design investigation for a SUPERSTAR small modular lead-cooled fast reactor demonstrator. Nucl Eng Des 2011;241:3021–31.
[24] Li H, Huang X, Zhang L. Operation and control simulation of a modular high temperature gas cooled reactor nuclear power plant. IEEE Trans Nucl Sci 2008;55:2357–65.
[25] Halimi B, Suh KY. Computational analysis of supercritical CO_2 Brayton cycle power conversion system for fusion reactor. Energy Convers Manage 2012;63:38–43.
[26] Oka Y, Koshizuka S, Ishiwatari Y, Yamaji A. Super light water reactors and super fast reactors. New York: Springer; 2010.
[27] Tsvetkov P. Nuclear Power-System Simulations and Operation. Croatia: InTech; 2011.
[28] Shtessel YB. Sliding mode control of the space nuclear reactor system. IEEE Trans Aerosp Electron Syst 1998;34:579.
[29] Upadhyaya BR, Zhao K, Xu X. Autonomous control of space reactor systems. Annual Report prepared for the U.S. Department of Energy NEER Program; 2005.
[30] Rowen WI. Simplified mathematical representations of heavy duty gas turbines. Trans ASME, J Eng Power 1983;105:865.
[31] Hajagos LM, Berube GR. Utility experience with gas turbine testing and modeling. IEEE Power Engineering Society Winter Meeting 2001;2:671–7.
[32] Bagnasco A, Delfino B, Denegri GB, Massucco S. Management and dynamic performances of combined cycle power plants during parallel and islanding operation. IEEE Trans Energy Convers 1998;13:194–201.
[33] Undrill J, Garmendia A. Modeling of combined cycle plants in grid simulation studies. IEEE Power Eng Soc Winter Meet 2001;2:657–63.
[34] Centeno P, Egido I, Domingo C, Fernandez F, Rouco L, Gonzalez M. Review of gas turbine models for power system stability studies. In: 9th Spanish Portuguese Congress on Electrical Engineering, Spain; 2005.
[35] Yee SK, Milanovic JV, Hughes FM. Overview and comparative analysis of gas turbine models for system stability studies. IEEE Trans Power Syst 2008;23:108–18.
[36] Chacartegui R, Sánchez D, Muñoz A, Sánchez T. Real time simulation of medium size gas turbines. Energy Convers Manage 2011;52:713–24.
[37] Suzuki N, Shimazu Y. Reactivity-initiated-accident analysis without scram of a molten salt reactor. J Nucl Sci Technol 2008;45:575.
[38] Hetrick DL. Dynamics of nuclear reactors. American Nuclear Society; 1993.
[39] Duderstadt JJ, Hamilton LJ. Nuclear reactor analysis. John Wiley & Sons; 1976.
[40] McAllister EW. Pipeline rules of thumb handbook: quick and accurate solutions to your everyday pipeline problems. Gulf Professional Publishing; 2009.
[41] Lamarsh JR, Baratta AJ. Introduction to nuclear engineering. 3rd ed. Prentice Hall; 2001.
[42] Agency IAE. Nuclear power plant design characteristics: structure of nuclear power plant design characteristics in the IAEA Power Reactor Information System (PRIS). Vienna: Intl Atomic Energy Agency; 2007.
[43] Hess GK, Demuth HB, Brown EA, Mohler RR. Control systems for the KIWI-A nuclear reactors. IRE Trans Nucl Sci 1962;9:134–44.
[44] Karassik IJ, Messina JP, Cooper P, Heald CC. Pump Handbook. 3rd ed. McGraw-Hill Professional; 2000.
[45] Love J. Process automation handbook: a guide to theory and practice. Springer; 2007.
[46] Lipták BG. Instrument engineers' handbook: process control. CRC Press; 1995.
[47] Abbasov N, Zeinalov R, Azizova O, Imranova S. Dynamic models of heat exchangers. Chem Technol Fuels Oils 2006;42:25–9.
[48] Tavakoli MRB, Vahidi B, Gawlik W. An educational guide to extract the parameters of heavy duty gas turbines model in dynamic studies based on operational data. IEEE Trans Power Syst 2009;24:1366–74.
[49] Najjar YSH. Some trends and progress in gas turbine technology and research. Energy Convers Manage 1996;37:1713–23.
[50] Murty PSR. Operation and control in power systems. Second. CRC Press; 2008.
[51] Shayeghi H, Shayanfar HA, Jalili A. Load frequency control strategies: a state-of-the-art survey for the researcher. Energy Convers Manage 2009;50:344–53.
[52] Ignatiev V, Feynberg O, Gnidoi I, Merzlyakov A, Smirnov V, Surenkov A, et al. Progress in development of Li, Be, Na/F molten salt actinide recycler & transmuter concept. In: Proceedings of ICAPP 2007, Nice, France; 2007.
[53] Merle-Lucotte E, Heuer D, Allibert M, Doligez X, Ghetta V, LeBrun C. Optimization and simplification of the concept of non-moderated thorium molten salt reactor. Switzerland: Int. Conf. Physics of Reactors; 2008.
[54] Mitachi K, Okabayashi D, Suziki K, Yoshida R. The re-evaluation of the nuclear characteristics of the small molten salt reactor. J AESJ 2000;42:936.
[55] Furukawa K, Arakawa K, Erbay LB, Ito Y, Kato Y, Kiyavitskaya H, et al. A road map for the realization of global-scale thorium breeding fuel cycle by single molten-fluoride flow. Energy Convers Manage 2008;49:1832–48.
[56] Sabharwall P, Bragg-Sitton SM, Stoots C. Challenges in the development of high temperature reactors. Energy Convers Manage 2013.
[57] Engel JR, Bauman HF, Dearing JF, Grimes WR, McCoy HE, Rhoades WA. Conceptual design characteristics of a denatured molten-salt reactor with once-through fueling. TN (USA): Oak Ridge National Lab; 1980.
[58] Mourogov A, Bokov PM. Potentialities of the fast spectrum molten salt reactor concept: REBUS-3700. Energy Convers Manage 2006;47:2761–71.
[59] Bruynooghe C, Eriksson A, Fulli G. Load-following operating mode at Nuclear Power Plants (NPPs) and incidence on Operation and Maintenance (O&M) costs, compatibility with wind power variability. Luxembourg: European Union; 2010.